Composites Part B 310 (2026) 113118

Contents lists available at ScienceDirect

Composites Part B

journal homepage: www.elsevier.com/locate/composites

Manufacturing of ultra-thin thermoplastic TRAC longerons

J. Koord [a,b,*], F. Benazzo [b], C. Hühne [a], S. Pellegrino [b]

[a] German Aerospace Center (DLR), Institute of Lightweight Systems, Lilienthalplatz 7, 38108 Braunschweig, Germany
[b] Graduate Aerospace Laboratories, California Institute of Technology, 1200 E. California Bvd., 91125 Pasadena, CA, USA

ARTICLE INFO

Keywords:
Thermoplastic composites
Thin-ply prepreg
Out-of-autoclave processing
Deployable structures

ABSTRACT

Deployable composite structures such as TRAC (Triangular Rollable and Collapsible) longerons are highly attractive for large-scale space applications due to their compact stowage and passive deployment capabilities. Conventional TRAC longeron manufacturing relies on autoclave-cured thermoset composites, which limits scalability. This study presents an out-of-autoclave manufacturing approach for ultra-thin thermoplastic longerons using thin-ply PEEK-based prepreg systems. A modular 3-step process (comprising laminate consolidation, web welding, and flange shaping) is applied to evaluate the effects of processing parameters and prepreg quality. Laminates are assessed via mechanical testing, computed tomography (CT), differential scanning calorimetry, and thermogravimetric analysis, revealing that fiber distribution homogeneity and thickness control are critical for void suppression, forming behavior, and overall laminate quality. Complete longerons are manufactured and analyzed using high-resolution laser scanning and CT analysis. Shape accuracy is found to strongly correlate with laminate uniformity, with flange radius deviations of up to 48% being observed in materials with poor fiber architecture. The most uniform prepregs yield nearly cylindrical flanges and geometric distortion of less than 10%. These results demonstrate that, with careful process control and prepreg selection, out-of-autoclave manufacturing can achieve structural and geometric quality comparable to autoclave-based production, enabling scalable fabrication of deployable composite structures.

1. Introduction

For decades, deployable structures have been used in spacecraft design as they allow for efficient packaging of large structures in order to comply with tight volume constraints of launch vehicles. An example is coilable structures, in which the cross-section is elastically flattened to enable coiling around a cylindrical hub for efficient packaging (see Fig. 1). Deployable booms based on coiling not only possess high packaging efficiency but are also able to deploy passively by releasing their stored elastic strain energy, which makes them attractive for application in ultra lightweight structures. They are commonly used in large deployable antennas [1], solar arrays [2,3], and solar sails [4,5].

The standard tape spring is the most basic example of a coilable boom, however, other designs that offer superior mechanical performance include the Storable Tubular Extendible Member (STEM) [6], the Collapsible Tube Mast (CTM) [7,8], and the SHEARLESS boom [9]. A coilable boom design with arguably yet superior properties is the Triangular Rollable And Collapsible (TRAC) boom. The concept was first introduced by Banik and Murphey [10]. Fig. 1 illustrates the TRAC boom cross-section, which is made up of two circular arcs (tape springs) connected along one edge to form a flat web and two curved flanges. Despite the open cross-section of the TRAC geometry, which is responsible for much lower torsional stiffness than CTM booms, its compact cross-sectional design allows for high bending-stiffness to packaged-height ratio, which leads to an efficient overall design [11].

TRAC booms made from metal alloys have been successfully used for in-orbit deployment of large solar sail demonstrators, namely NASA's NanoSail-D [12,13] as well as the Planetary Society's LightSail-1 [14] and LightSail-2. Recently, TRAC longerons have been used as components of large structures made from thermoset based Carbon Fiber Reinforced Polymers (CFRP). Composite materials not only offer mechanical advantages in order to further increase packing efficiency but are also less sensitive to thermal gradients, which otherwise cause large deflections when a metallic structure is only partly facing the sun [15]. Application of ultra-thin thermoset CFRP longerons has been successfully demonstrated in the DOLCE (Deployable on-Orbit ultra-Light Composite Experiment) technology demonstration, as part of the Caltech Space Solar Power Project (SSPP) mission SSPD-1 [16,17]. In Fig. 2, TRAC longerons form the edges of the trapezoidal modules, measuring up to 1.7 m in length. They are composed of a seven-ply

* Corresponding author at: German Aerospace Center (DLR), Institute of Lightweight Systems, Lilienthalplatz 7, 38108 Braunschweig, Germany.
E-mail address: josef.koord@dlr.de (J. Koord).

https://doi.org/10.1016/j.compositesb.2025.113118
Received 10 August 2025; Received in revised form 13 October 2025; Accepted 19 October 2025
Available online 22 October 2025

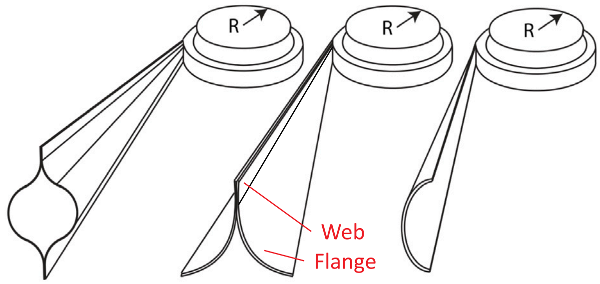

Fig. 1. CTM, TRAC and standard tape spring boom concepts partially coiled around a cylindrical hub [22].

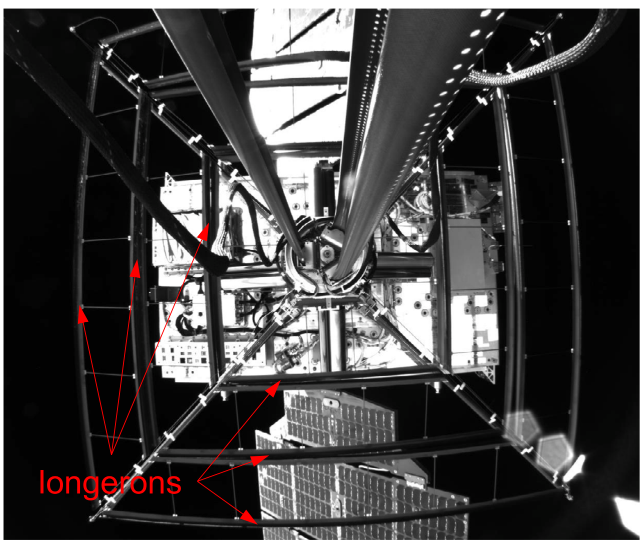

Fig. 2. TRAC longerons in the DOLCE technology demonstrator following on-orbit deployment during the SSPD-1 mission.

layup cured in an autoclave process using thin-ply thermoset CFRP and GFRP prepregs. This results in a web and flange thickness of only 185 μm and 80 μm, respectively, which is thin enough to be tightly coiled around the deployment mechanism while still providing the required deployed stiffness. While the DOLCE structure in the SSPD-1 mission measured 1.7 m × 1.7 m, future development stages envision a full size of around 60 m × 60 m [18]. At such scales, manufacturing of parts in an autoclave process becomes more and more challenging due to the size constraints of even the largest autoclaves currently available. Other projects aiming at developing ultra-large structures (> 100 m) [19–21], are facing similar challenges.

One way to overcome the size limitations of traditional composite structures is to transition from thermoset (TS) based CFRP, cured in an autoclave process [23], to thermoplastic (TP) matrix systems. Thermoplastic CFRP (CFRTP) prepregs can be consolidated in an out-of-autoclave process through the localized application of heat and pressure, and subsequently formed into the desired TRAC geometry using the same principles. This approach enables the quasi-continuous fabrication of longerons with virtually no restriction on length. In the context of in-space manufacturing and assembly, the concept can be extended even further: TP boom components can be prefabricated on Earth and welded in orbit, allowing the construction of ultra-large structures that would otherwise be unfeasible. The latter concept is currently being explored by DLR and ESA through investigations into the in-space welding of CFRP truss structures [24].

Compared to the manufacturing of ultra-thin TRAC longerons using TS thin-ply CFRP prepreg, the transition to TP-based systems poses multiple challenges. First, the production of thin-ply prepreg impregnated with TP matrices is more difficult due to the higher viscosity and processing temperatures of TP systems like polyether ether ketone (PEEK) compared to TS matrices like epoxy resins [25,26]. As a result, TP thin-ply prepreg currently lags behind its TS counterparts not only in terms of minimum achievable ply thickness, but also in the uniformity of fiber distribution and tape thickness [27,28]. Furthermore, consolidation of CFRTP is more demanding with respect to laminate quality and shape conformity of the final structure (e.g. TRAC longerons). In particular, the combination of high melt temperatures, elevated viscosity, and complex polymer crystallization behavior present major challenges in processing TP matrix systems into ultra-thin composite structures [22,27,29].

Schlothauer et al. [22,28] avoided the use of thin-ply TP prepreg by using a film stacking process in a hot-press for the impregnation and consolidation of dry carbon fiber spread-tow with PEEK in a one step process. Very low single-ply thicknesses of around 35 μm were achieved with a void content of around 1% at a fiber volume fraction (FVF) of around 50%. The laminate thicknesses in the study range between 100–150 μm. In addition to demonstrating the feasibility of thin shell laminates made of thin-ply CFRTP, an increase in transverse tensile strength was observed, which constitutes yet another advantage over TS-based thin-ply laminates. To the best knowledge of the authors, this is the only study of thin shell laminates based on thin-ply CFRTP, which highlights the necessity to build a better understanding of this class of structures.

Currently, TRAC longerons are manufactured using TS-based thin-ply prepreg material in an autoclave process [23]. Ultimately, the goal is to manufacture TRAC longerons using TP-based thin-ply prepreg via a continuous consolidating, welding, and shaping process. Since substituting both the material and manufacturing process requires significant technological advancements, the development has been organized into three distinct phases. The first step involves switching from TS to TP materials while retaining the autoclave process, as detailed in Benazzo and Pellegrino [30]. The second step, discussed in the present paper, shifts from autoclave manufacturing of TP-based TRAC longerons to an out-of-autoclave process. This involves consolidating single TP thin-ply layers in a press, welding the TRAC web in a press, and shaping the flanges in an oven. In the third and final step, the transition to a unified quasi-continuous manufacturing process for the production of ultra-long TRAC structures will be completed in a future study.

As part of the second development step, transitioning to an out-of-autoclave process necessitates a thorough understanding of the thermoplastic consolidation behavior. In particular, the laminate quality of CFRTP produced by hot pressing strongly depends on the selected processing window. Key parameters include temperature, pressure, holding time, and cooling rate.

The following summarizes literature findings on the influence of these parameters for PEEK-based CFRTPs. The *processing temperature* has a primary influence, as it governs the melt viscosity of PEEK and thus its ability to impregnate the fiber bundles. Consolidation temperatures typically exceed the melting point of PEEK (343 °C) [31], with optimal molding windows reported between 360 °C and 400 °C [32–35]. Within this range, a balance must be maintained: while increasing temperature reduces viscosity and enhances flow, values above 400 °C can lead to oxidative crosslinking and thermal degradation of the polymer chains, increasing viscosity over time and impeding resin infiltration [36]. These effects directly impact void formation and mechanical performance [35,37,38]. *Processing pressure* is equally critical. Pressures between 2 and 3.5 MPa have been shown to promote adequate resin flow and air evacuation, thereby reducing porosity and improving interfacial bonding [31,35]. However, excessive pressure may lead to resin starvation or fiber washout, causing fiber–matrix debonding and non-uniform consolidation. A pre-pressing stage at sub-melting temperatures has been reported to improve gas evacuation prior to resin flow [31,39]. A *dwell time* between 20 and 30 min at the processing temperature enables complete fiber wetting, but longer dwell times accelerate PEEK degradation, increasing brittleness and reducing mechanical strength [31,32,35]. The *cooling rate* after consolidation significantly affects crystallization. Slow cooling promotes higher crystallinity and more stable morphology, whereas rapid cooling results in lower crystallinity, reduced matrix stiffness, and poorer fiber–matrix adhesion [29,40]. All key processing parameters influence not only crystallinity and void formation, but also the development of residual stresses and the quality of the fiber–matrix interface. Elevated void contents (above 1.2%), accumulated thermal stresses, and poor interfacial bonding often resulting from sub-optimal processing, have been shown to degrade matrix-dominated properties and impair stress transfer, ultimately reducing mechanical performance [40–42].

While existing studies provide insight into individual consolidation parameters, they often focus on thicker laminates or conventional layups. The behavior of ultra-thin TP-based laminates, particularly in the context of shaping TRAC longerons, remains insufficiently explored. The present study addresses this gap by characterizing advanced PEEK-based thin-ply prepreg systems and evaluating their suitability for TRAC longeron manufacturing. A modular process is developed that isolates the key steps of (i) laminate consolidation, (ii) web welding, and (iii) TRAC shaping. The influence of processing parameters on laminate quality is assessed through differential scanning calorimetry (DSC), thermogravimetric analysis (TGA), high-resolution computed tomography (CT), and mechanical testing. Finally, TRAC longerons are manufactured and their geometric accuracy and internal microstructure are analyzed in detail using laser scanning and CT imaging, respectively. The findings provide a foundation for advancing scalable, out-of-autoclave manufacturing strategies for ultra-lightweight composite structures targeted towards future space applications.

2. Materials and manufacturing

There are several choices of thermoplastic matrices suitable for space applications, including PEEK, polyphenylene sulfide (PPS), polyaryletherketone (PAEK), and polyimides, each offering unique advantages for specific use cases (see Table 1). Among these, PEEK is an ideal candidate for the manufacturing of high-performance longerons due to its promising combination of mechanical, thermal, and environmental properties. Its excellent thermal stability ensures reliable performance across temperature fluctuations [43,44]. PEEK exhibits minimal outgassing [45,46], a critical requirement for vacuum compatibility, and has proven resistance to radiation and chemical degradation [47,48], ensuring long-term durability in harsh conditions.

Therefore, three different semi-crystalline PEEK-based prepreg systems are investigated within the present study: (i) UD-CFRTP tape (hereafter referred to as FK) based on T700 fibers and PEEK with a nominal tape thickness of 60 μm, a tape width of 80 mm and a FVF of 60% provided by FUKUVI Chemical Industry Co., Ltd. and Industrial Technology Center of Fukui prefecture, that originally developed the tow spreading technology [49]; (ii) UD-CFRTP tape (hereafter referred to as SH) by SHINDO Co., Ltd. using CF and PEEK with a nominal tape thickness of 58 μm, a tape width of 195 mm and a FVF of 57%; (iii) UD-CFRTP tape (hereafter referred to as XX) by a different manufacturer using M30SC and PEEK with a tape thickness of 55 μm, a tape width of 60 mm and FAW of 38 gsm.

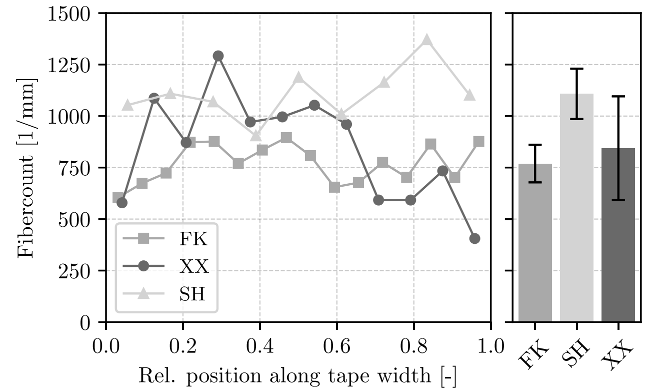

Fig. 3. Fibercount along tape width and mean value incl. standard deviation for each CFRTP prepreg tape (FK, SH, XX).

As the manufacturers' data-sheets contain no information on the degree of crystallinity of the PEEK in each prepreg, DSC measurements were conducted on the raw tape material. The results indicated that all materials have a relatively high degree of crystallinity to begin with, especially in case of XX (see Table 2), which might influence the subsequent processing of the material.

2.1. Thermoplastic thin-ply tape quality

Before manufacturing any laminates, the tape quality was analyzed in order to get a better understanding of the materials in use. For this purpose, 5 mm wide cutouts were taken from the raw tape and analyzed using X-ray micro-computed tomography (μCT) in a Xradia Versa XRM-510. In the case of FK, for example, the 80 mm wide tape was divided into 16 cutouts. For XX and SH, 12 and 9 cutouts along the width were analyzed, respectively. The homogeneity of the tape was quantified on the basis of the fibercount, i.e. the number of fibers per unit length. Fig. 3 shows the fibercount of the three prepreg tapes normalized along their width. XX exhibits the largest spread in fibercount along the tape width, i.e. is less homogeneous than FK and SH. This observation is confirmed by the means and standard deviations along a section of the tapes, presented in Fig. 3, where XX shows the highest standard deviation, while the standard deviations for FK and SH are of similar magnitude. Compared to FK and XX, SH has a higher fibercount per unit length at similar tape thicknesses, which reflects the higher FAW as depicted in the material data sheet in Table 2.

In Fig. 4, the CT images of all three tapes are presented at the position of highest and lowest fibercount, respectively. At first glance, the quantitative observations regarding homogeneity are qualitatively confirmed by the images. FK shows the highest homogeneity in both fiber and thickness distribution, followed by SH and eventually XX, which exhibits rather poor homogeneity regarding both fibercount and tape thickness. This indicates that, despite achieving the lowest FAW, the XX material exhibits drawbacks in tow-spreading and PEEK impregnation. Further observation of Fig. 4 reveals a deeper insight into the tape manufacturing process. According to the manufacturer, the FK tape's architecture consists of 3 PEEK sheets and 2 CF tow-spreads (PEEK/CF/PEEK/CF/PEEK), which can be seen quite clearly in Fig. 4(b). Similarly, the composition of SH (CF/PEEK/CF) can be drawn from the CT images (see Fig. 4(c) and Fig. 4(d)), as all the fibers are present on the edge of a thin central matrix layer. In the case of XX, however, the prepreg architecture is not clear.

Regarding material handling during manufacturing, the FK tape is advantageous due to its smooth, glossy surface. In contrast, the

Table 1
Comparison of high-performance thermoplastic materials for space application.

	PEEK Polyether Ether Ketone	PAEK Polyaryletherketone	PES Polyethersulfone	PEI Polyetherimide	PPS Polyphenylene Sulfide	PPSU Polyphenylsulfone
Thermal Stability	Up to 250 °C	Up to 250 °C	Up to 180 °C	Up to 200 °C	Up to 260 °C	Up to 220 °C
Outgassing	Very Low	Low	Moderate	Very Low	Very Low	Very Low
Radiation Resistance	Excellent	High	Moderate	Moderate	High	High
Mechanical Strength	High	High	Moderate/High	High	High	Moderate/High
Chemical Resistance	Excellent	Excellent	Good	Excellent	Excellent	Excellent

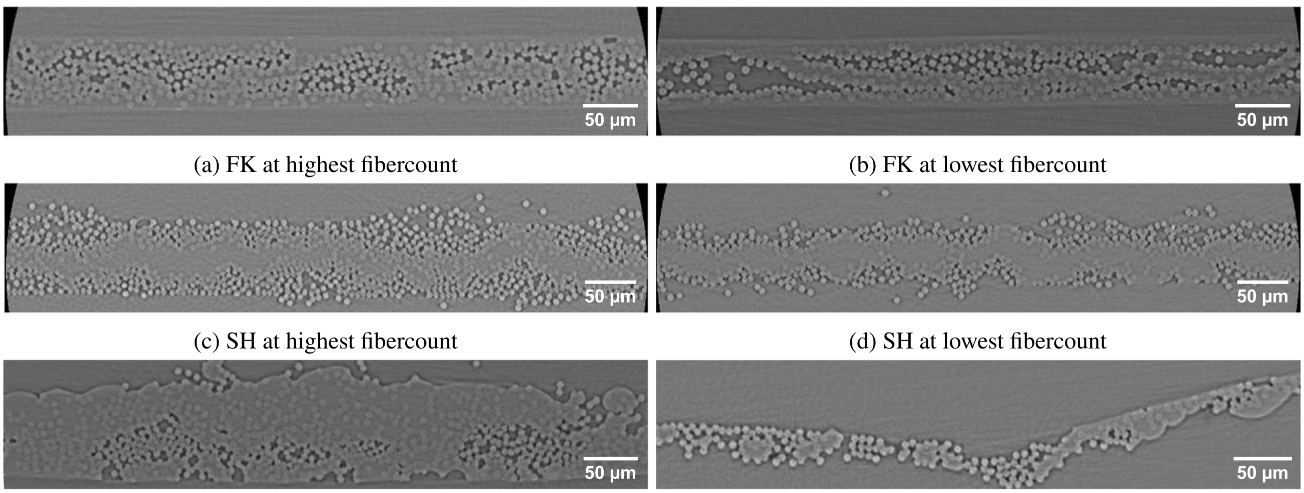

(a) FK at highest fibercount (b) FK at lowest fibercount

(c) SH at highest fibercount (d) SH at lowest fibercount

(e) XX at highest fibercount (f) XX at lowest fibercount

Fig. 4. Comparison of prepreg tape homogeneity using CT scans.

Table 2
Datasheet information on thermoplastic thin-ply prepreg tape.

	Unit	FK	SH	XX
Fiber	–	T700 (HS)	CF	M30SC (IM)
Matrix	–		semi-crystalline PEEK	
Crystallinity[a]	%	28.6 ± 1.0	23.7 ± 1.1	32.2 ± 2.1
FAW	gsm	48	57	38
FVF[b]	%	47.8 ± 0.6	54.2 ± 1.2	43.0 ± 2.2
Thickness[c]	μm	60	58	55
Tape width	mm	80	195	60

[a] Determined by DSC.
[b] Determined by TGA.
[c] Measured by caliper.

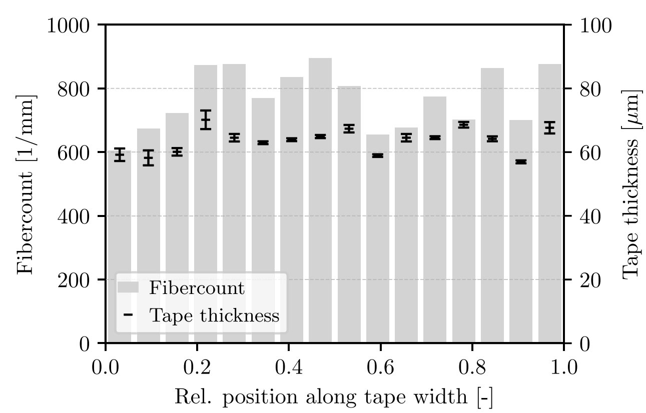

Fig. 5. Fibercount and tape thickness measured by CT along tapewidth.

SH tape exhibits a number of loosely attached, unimpregnated fibers on the surface, which complicate processing and can lead to fiber misalignment. In case of the XX tape, the locally low fibercount in conjunction with low laminate thickness and poor impregnation (see Fig. 4(f)) can lead to rupture of the tape during handling as well as highly uneven laminates after consolidation.

Fig. 5 provides further insight into the quality of the FK tape. Both fibercount and tape thickness are derived from CT scans. While the fibercount (770 ± 91 fibers/mm) exhibits a coefficient of variance (CV) of 11.9%, the tape thickness (64 ± 4 μm) has a CV of 5.9%. These results suggest that improving homogeneity in the FK tape may be more effectively achieved by enhancing tow spreading rather than modifying the impregnation process. A comparable analysis could not be performed for the other laminates due to the absence of a well-defined edge for thickness measurement.

2.2. Manufacturing process

To ensure accurate geometric shaping and laminate quality in the manufacturing of ultra-thin TRAC longerons, the final continuous production sequence was divided into discrete stages that can be independently varied and analyzed using a hot-press and oven setup. This modular approach enables a systematic investigation of how key processing parameters (e.g. temperature, pressure, dwell time, and cooling rate) affect laminate integrity and dimensional conformity. As explained previously (see Fig. 6), a three-step manufacturing strategy was adopted, consisting of (i) laminate consolidation, (ii) web welding, and (iii) TRAC shaping. This separation allows material-related effects

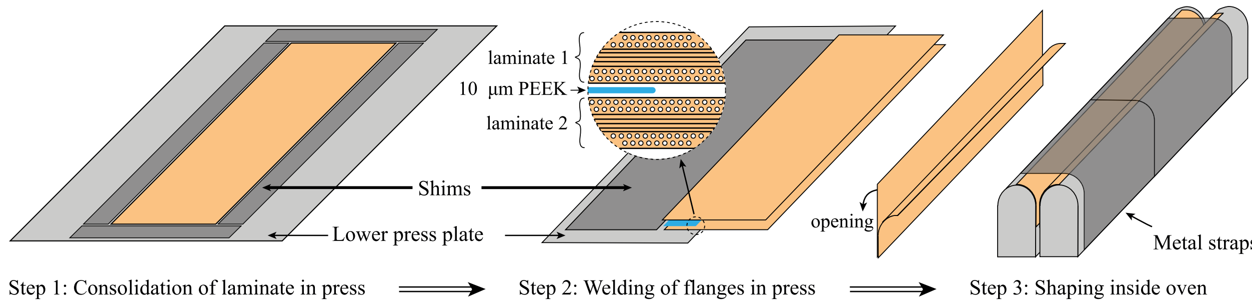

Fig. 6. Three-step process for manufacturing TRAC longerons.

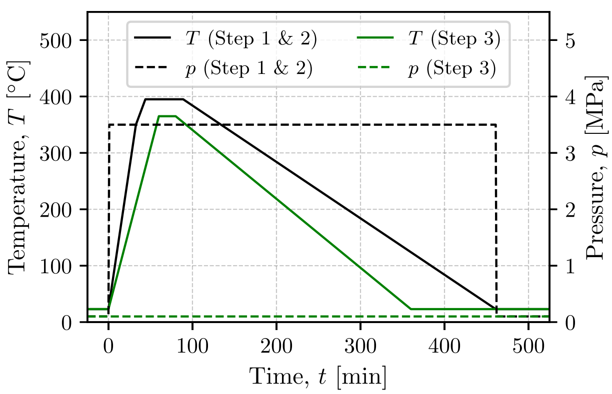

Fig. 7. Nominal process parameters for consolidation (Step 1), welding (Step 2) and shaping (Step 3).

to be isolated from process-induced instabilities associated with quasi-continuous operation. Manufacturing was conducted using a LabPro 200 hot-press (Fontijne Presses), which provides a maximum closing force of 200 kN and a maximum plate temperature of 500 °C, and a Grieve HT-800 industrial oven, with a maximum operating temperature of 450 °C.

Step 1: Consolidating laminates in hot-press

UD plies were stacked to form a symmetric cross-ply laminate with a [0, 90, 0] layup and inserted into the press. The laminate for manufacturing the longerons is 45 mm × 195 mm, separated from the press by polyimide foil of 50 µm in thickness (not shown in Fig. 6). The laminate thickness was controlled using steel shims. Prior to placement into the press, release agent was applied on the polyimide foil and steel shims. The nominal temperature T and pressure p for the consolidation cycle are presented in Fig. 7. The final process parameters were selected through the parametric study presented in Section 2.3. The heating and cooling rates were set to constant values of 10 °C/min and 2 °C/min, respectively. In order to avoid a temperature overshoot, the heating process was decreased to a rate of 5 °C/min starting 350 °C.

Step 2: Welding of flanges in hot-press

A large square shim of 200 mm × 200 mm was placed in the center of the press plate in order to control the thickness of the web area (300 µm) as well as to ensure a symmetrical load distribution under the press plates. The straight edge of the shim simultaneously serves as a dam to prevent matrix flow and avoid deformations of the welded plies. Two consolidated cross-ply laminates with one layer of PEEK film (10 µm) were placed at the edge of the press plate against the center shim and fixed using polyimide tape. The cycle step 1 was applied to weld the web area which is defined by the PEEK film, resulting in a six-ply laminate that is connected in the web area and separated in the flange area, as shown in Fig. 6.

Step 3: Shaping inside oven

In this step, the welded flanges were formed into the final TRAC longeron shape by inserting the laminate into an aluminum mold and clamping the web area between the two parallel faces of the mold. The flanges were opened and fixed onto the aluminum mold with high temperature Kapton tape. Steel straps were wrapped around the setup to both apply a radial force on the laminate during heating, and improve the surface finish. Shaping was done for 20 min at 365 °C.

2.3. Consolidation parameters

Several studies have investigated the consolidation behavior of CF/PEEK materials, with particular emphasis on processing temperature, dwell time, and applied pressure [31,32,34,35]. Based on findings from the literature, a baseline processing configuration for the FK material was defined, comprising a shim thickness of 150 µm, a maximum processing temperature of 405 °C, a dwell time of 30 min, and an applied pressure of 3.5 MPa. Each parameter was varied individually, and its effect on the resulting laminate quality was systematically investigated. A total of 10 laminates with a cross-ply layup [0, 90, 0] and measuring 80 mm × 160 mm were consolidated. The results of this parametric study on FK are presented in the following. A summary of the final selected processing parameters for all three material systems is provided in Table 4.

2.3.1. Variation of shim thickness

Based on the prepreg tape thickness of FK (60 µm) and a 3-ply layup, a shim thickness of 150 µm is selected as baseline to control laminate thickness, ensure uniform pressure distribution and void-free consolidation as well as good interlaminar bonding. Additional shim thicknesses of 130 µm, 175 µm, and 200 µm are tested at otherwise constant parameters (T = 400 °C, t_{dwell} = 30 min, and p = 3.5 MPa).

Fig. 8(a) shows the effect of the shim thickness on the resulting laminate. As expected, decreasing the shim thickness resulted in a smaller laminate thickness. However, the evenness of the laminate was also negatively affected, as the thickness variation within the laminate increased. A shim thickness of 175 µm was found to exhibit the least variance in measured laminate thickness as well as the cured ply thickness (CPT) in Table 3.

In Fig. 9, CT scans are presented for the laminates consolidated using different shim thicknesses. While the shim thicknesses of 130 µm and 150 µm resulted in very high laminate quality and low void content, it can be seen that consolidation with 175 µm and 200 µm shims leads to areas with large voids. Here, it appears that a shim thickness of 150 µm or lower is a good choice regarding laminate quality. Analysis of the fiber volume fraction (FVF) in Table 3 correlates well with the qualitative observations regarding laminate quality from Fig. 9. A slight increase in FVF was observed with decreasing shim thickness, suggesting resin depletion from the laminate due to either

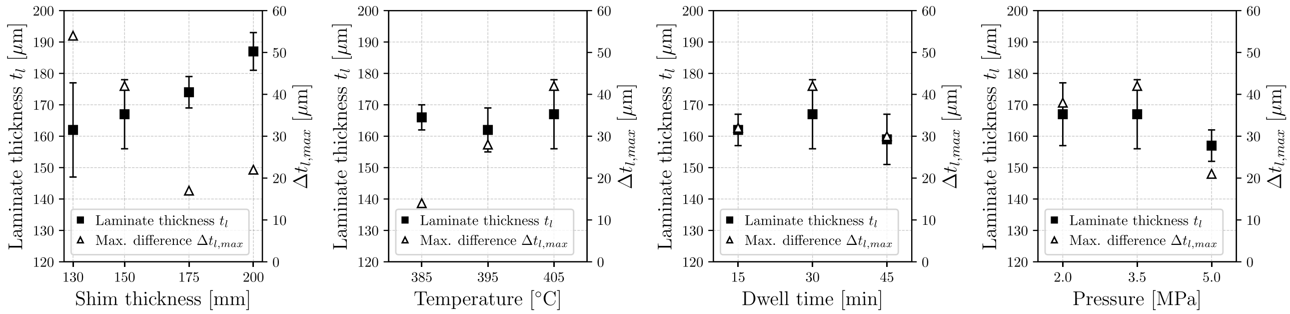

(a) (b) (c) (d)

Fig. 8. Effect of variation of consolidation parameters on laminate thickness t_l and maximum thickness difference within a laminate $\Delta t_{l,max}$.

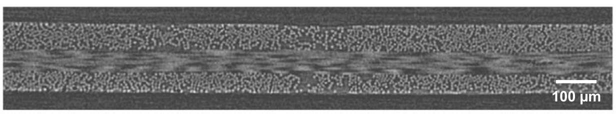

(a) Shim thickness of 130 µm

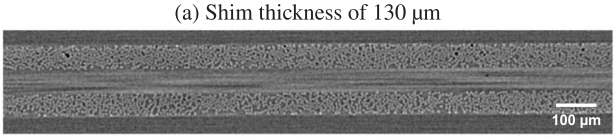

(b) Shim thickness of 150 µm

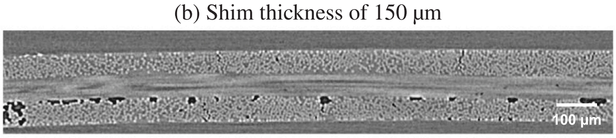

(c) Shim thickness of 175 µm

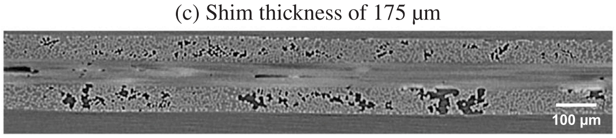

(d) Shim thickness of 200 µm

Fig. 9. Effect of shim thickness on laminate quality based on CT scans for constant parameters (T=405 °C, t_{dwell}=30 min, and p = 3.5 MPa).

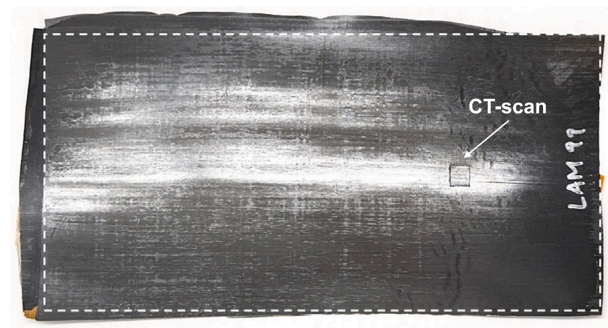

(a) Lateral deformation due to low shim thickness of 130 µm

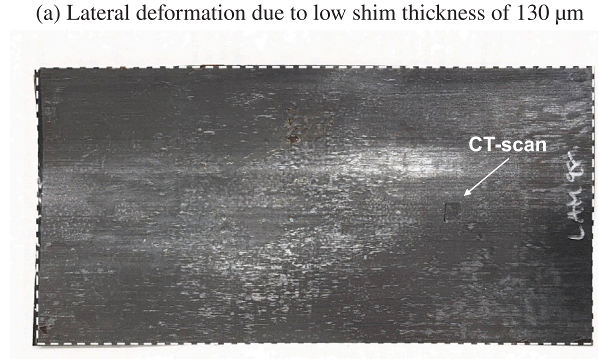

(b) Good shape conformity for shim thickness of 200 µm

Fig. 10. Photograph of laminate top side after consolidation (T=405 °C, t_{dwell}=30 min, and p = 3.5 MPa; nominal laminate size 80 mm × 160 mm).

enhanced squeeze-out during the consolidation process or fiber and matrix migration, increasing the overall laminate's surface area.

This increase in laminate surface was corroborated with a visual analysis of the laminate, Fig. 10, which reveals that laminates with very low shim thicknesses (150 µm and below) exhibit substantial lateral deformation, or "squishing", during consolidation. This behavior was likely caused by insufficient edge constraint, which allows for lateral displacement of the laminate when pressure is applied at the polymer's melting temperature. Since shape stability cannot be maintained under these conditions, the final shim thickness was selected as 175 µm based on a careful balance of competing factors, including thickness uniformity, laminate quality in terms of FVF and porosity, as well as overall shape conformity.

2.3.2. Variation of consolidation temperature

According to the published literature, processing temperatures for PEEK typically range from its melting point (343 °C) up to 415 °C [31]. Temperatures in the range of 380–400 °C are generally reported as suitable for achieving good consolidation quality [32,34,35]. However, temperatures exceeding 400 °C may offer additional benefits, particularly when paired with short thermal exposure times to mitigate the risk of thermal degradation [31,34]. In the context of a quasi-continuous manufacturing process, elevated temperatures combined with reduced dwell times may ultimately be necessary to maintain process efficiency while ensuring material performance. In the present study, 3 temperature levels were considered: 385 °C, 395 °C, and 405 °C for otherwise constant parameters (t_{shim} = 150 µm, t_{dwell} = 30 min, and p = 3.5 MPa).

Fig. 8(b) indicates that higher processing temperatures lead to a higher scatter in laminate thickness distribution, likely due to the decrease in viscosity of the matrix at higher temperatures [31]. A lower processing temperature yields better uniformity but void content is slightly increasing. Comparison of crystallinity in Table 3 shows very similar values for laminates consolidated at 385 °C (31.5%) and 395 °C (30.9%). Increasing the consolidation temperature to 405 °C further raises crystallinity to 34.8%. For reference, the initial prepreg crystallinity was approximately 28%. The increase at 405 °C can likely

Table 3
Cured ply thickness (CPT), crystallinity, and fiber volume fraction (FVF) of FK material for variation of shim thickness, temperature, and dwell time.

	Shim thickness [μm]	Temperature [°C]	Dwell time [min]	Pressure [MPa]	CPT [μm]	Crystallinity [%]	FVF [%]
FK prepreg (reference)	–	–	–	–	–	28.59 ± 1.01	47.8 ± 0.6
Variation of shim thickness	130	405	30	3.5	54.1 ± 5.2	30.22 ± 0.71	53.9 ± 0.7
	150	405	30	3.5	55.6 ± 3.7	34.79 ± 1.70	53.6 ± 0.9
	175	405	30	3.5	57.9 ± 1.6	33.93 ± 2.03	53.5 ± 0.7
	200	405	30	3.5	62.2 ± 1.8	33.50 ± 1.14	51.4 ± 0.5
Variation of temperature	150	385	30	3.5	55.4 ± 1.4	31.53 ± 1.23	–
	150	395	30	3.5	53.9 ± 2.5	30.93 ± 2.23	–
	150	405	30	3.5	55.6 ± 3.7	34.79 ± 1.70	–
Variation of dwell time	150	405	15	3.5	54.1 ± 2.8	27.43 ± 1.56	–
	150	405	30	3.5	55.6 ± 3.7	34.79 ± 1.70	–
	150	405	45	3.5	53.1 ± 2.8	31.84 ± 0.78	–

be attributed to the decrease in melt viscosity which enhances the polymer chain mobility at the higher temperature, thereby facilitating more complete melting and allowing for improved chain alignment and recrystallization during cooling. Furthermore, longer effective melting (even if dwell time is constant) at higher temperature can lead to more uniform melting of imperfect crystals, enabling better recrystallization [50,51]. A temperature of 395 °C was selected for processing, however, even higher temperatures were deemed acceptable as long as the dwell time remained short.

2.3.3. Variation of dwell time

Dwell times commonly investigated in the literature range between 10 min to up to 90 min. Generally, longer dwell times are beneficial for laminate quality [35] as well as mechanical performance [31]. In the present study, the dwell time was varied between 15 min, 30 min, and 45 min for otherwise constant parameters (t_{shim}=150 μm, T = 405 °C, and p = 3.5 MPa).

As shown in Fig. 8(c), varying the dwell time during consolidation had only a minor influence on the laminate's thickness distribution. However, the data in Table 3 reveals a notable effect on crystallinity: a dwell time of 15 min resulted in a crystallinity of 27.4%, which is comparable to that of the prepreg material (28.6%). In contrast, increasing the dwell time to 30 min and 40 min yielded significantly higher crystallinity levels. This suggests that at shorter dwell times, the material does not remain above the melting temperature long enough to reach the chain alignment needed to foster increased crystallinity during the cooling process. Instead, 30 min appear sufficient for the chain reorganization to take place, thereby enhancing crystal growth [50,52]. It should be noted that laminate squishing, as observed in Fig. 10, was present for the laminate with a longer dwell time as well. Thus, to balance the effects of crystal formation and laminate deformation, a dwell time of 30 min was selected.

2.3.4. Variation of pressure

The literature shows that too low pressure during consolidation results in poor interlaminar bonding and increased void-content, while excessive pressure can cause fiber wash-out or laminate distortion due to resin over-squeeze. Therefore, pressure must be cautiously selected as a compromise between void elimination and the risk of excessive matrix flow [53]. In general, moderate pressure between 3–4 MPa yield optimal laminate quality in terms of FVF, void content, and mechanical performance [32,34,53]. Pressure levels of 2 MPa, 3.5 MPa and 5 MPa were investigated at otherwise constant parameters (t_{shim} = 150 μm, T = 405 °C, and t_{dwell} = 30 min).

Fig. 8(d) demonstrates that a consolidation pressure of 5 MPa yielded favorable results in terms of laminate thickness uniformity, as the intra-laminate thickness variation was relatively low. Additionally, a slightly reduced overall thickness below 160 μm was achieved, which is beneficial for reducing coiling stresses in deployable longerons. However, it was also observed that a high consolidation pressure induces pronounced laminate distortion, comparable to the deformation seen in cases with insufficient shim thickness (see Fig. 10). While a low consolidation pressure of 2 MPa ensures good shape conformity, it is associated with a slightly elevated void content. Consequently, a pressure of 3.5 MPa was selected, again as a compromise, balancing reduced void formation with minimal laminate distortion.

Fig. 11. Setup for tensile testing.

2.4. Effects on mechanical properties

Thus far, the metrics used to infer the effects of processing parameters have focused on evaluating the laminates' morphology. However, determining the influence that these parameters have on the performance of these thin-ply materials is important. The greatest visual and microstructural differences were observed in the laminates with varying shim thickness, therefore these were selected for further analysis and prepared for tensile testing. Four samples of size 20 mm × 160 mm and with [0, 90, 0] layup were cut from each laminate and bonded to 20 mm × 30 mm tabs in accordance ASTM D3039. The samples were then clamped in a 5569 Instron universal testing machine equipped with a 50 kN load cell. The strain on the samples was measured using both a horizontal and a vertical laser extensometer by Electronic Instrument Research (EIR) with reflective tape targets on the tensile coupons (see Fig. 11). Mean and standard deviations were calculated for each group of samples and presented in Fig. 12.

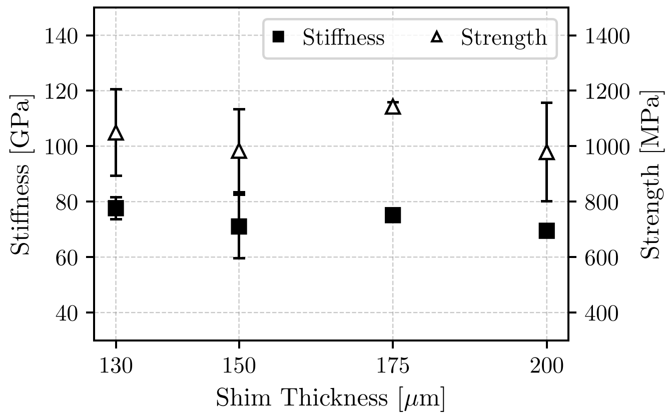

Fig. 12. Tensile test results for variation of shim thickness in FK for otherwise constant parameters (T=405 °C, t_{dwell}=30 min, and p = 3.5 MPa).

The tensile stiffness, shown in Fig. 12, increases from 69.5 GPa for the 200 μm shim to 77.6 GPa for the 130 μm shim. However, the standard deviation also increases as the shim thickness decreases. A similar trend is observed for tensile strength, which generally increases with decreasing shim thickness, though the associated standard deviations remain relatively high across all cases. These findings correlate well with the previously reported influence of shim thickness on laminate consolidation (see Fig. 8(a)) and underscore the critical role of shim selection in achieving both mechanical performance and manufacturing consistency. Thinner shims promote improved stiffness and strength by reducing the overall laminate thickness, yet are more susceptible to fiber misalignment and handling-induced defects, leading to higher variability. Conversely, thicker shims offer more robust processing but result in increased void content, which compromises the mechanical properties. It should be noted that the laminate produced with a 175 μm shim exhibited comparatively high stiffness and strength with low standard deviation, presenting an exception to the overall trend. Again, this suggests that a shim thickness of 175 μm offers a favorable balance between mechanical efficiency and manufacturing robustness.

2.5. Selection of processing parameters

Based on the considerations outlined in the previous section, the processing parameters summarized in Table 4 were selected for processing of the FK material. The selection reflects a balance of key factors, including laminate uniformity, crystallinity, void content, and shape stability as well as mechanical performance. Similar considerations guided the selection of processing parameters for the SH and XX materials, which are also presented in the table.

While FK and XX exhibit comparable stiffness in Table 4, SH is notably stiffer, likely due to its significantly higher FVF (see Table 2). FK shows the highest strength, followed by SH, while XX exhibits the lowest. In terms of scatter, FK displays a low standard deviation, whereas SH and XX exhibit considerably larger variations, particularly in terms of strength. The results suggest a potential influence of the prepreg quality on the mechanical performance of the [0, 90, 0] laminates. However, differences in fiber type and content between the materials limit the direct comparability of these results.

The corresponding CT images illustrating the laminate quality for these materials are shown in Fig. 13. The SH material exhibits excellent laminate quality, characterized by a homogeneous fiber distribution, consistent single-ply thickness, and low void content. In contrast, the XX material shows significantly reduced quality across these metrics. Further optimization of the processing parameters was not considered promising, as the observed deficiencies are attributed primarily to the quality of the base prepreg material (see Fig. 4) rather than to the selected processing conditions. This concludes the investigations on the processing parameters at the laminate level. In the following, TRAC longerons are investigated at the structural level.

Table 4
Final consolidation parameters and mechanical properties.

	Unit	FK	SH	XX
Shim Thickness	μm	175	175	150
Temperature	°C	395	405	395
Dwell Time	min	30	30	30
Pressure	MPa	3.5	3.5	3.5
Stiffness	GPa	75.1 ± 2.3	101.1 ± 7.9	71.1 ± 12.6
Strength	MPa	1143 ± 16	948 ± 138	883 ± 205

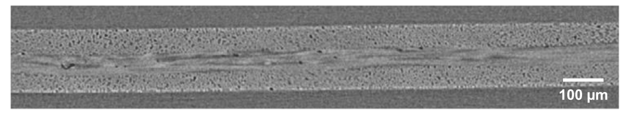

(a) SH material

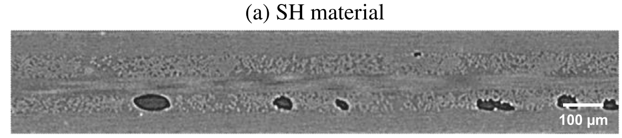

(b) XX material

Fig. 13. CT scans of SH and XX laminates made with final consolidation parameters.

3. Analysis of TRAC longerons

3.1. Manufacturing

By applying the process parameters determined in the previous section (see Table 4), three TRAC longerons were manufactured using FK, XX, and SH thin-ply TP prepreg material. The 3-step process outlined in Fig. 6 was applied to all three longerons and the resulting structures are presented in Fig. 14.

Upon visual inspection, the FK-based TRAC longeron in Fig. 14(a) displays a smooth, glossy surface across both flanges and the web, indicating good impregnation and consolidation. The web edge appears clean and well-defined, and only slight surface waviness is present. A few small (<1 mm) white areas are visible, which may correspond to localized voids or regions of incomplete fiber wetting, though they appear infrequent and non-critical. In contrast, the XX specimen in Fig. 14(c) exhibits a significantly higher number of white surface areas and more pronounced flange waviness, likely indicative of less uniform consolidation and prepreg quality. A noticeable twist of the web along the longitudinal axis is also observed, possibly resulting from residual stress buildup or asymmetric laminate properties. The SH longeron in Fig. 14(b), on the other hand, presents a matte surface finish with distinct rough regions, which is visibly different from both FK and XX. Despite this, its overall shape is good, with only minor flange waviness. These macroscopic observations are consistent with the CT and handling-based findings discussed in Section 2.3 and suggest that differences in prepreg quality and consolidation behavior contribute to the observed variation in laminate quality and shape of the longerons.

3.2. Shape accuracy

To quantitatively assess the geometry of the manufactured longerons and compare the influence of different thermoplastic prepreg systems,

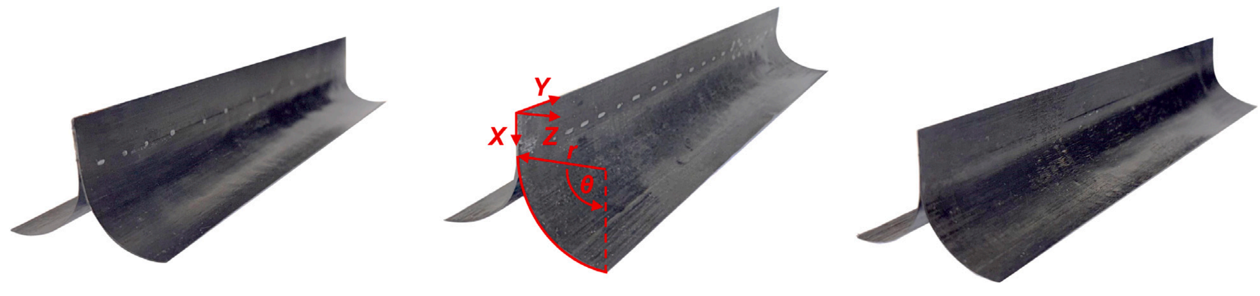

(a) FK longeron (b) SH longeron (c) XX longeron

Fig. 14. Photographs of TRAC longerons made from different TP thin-ply prepreg systems in 3-step manufacturing process.

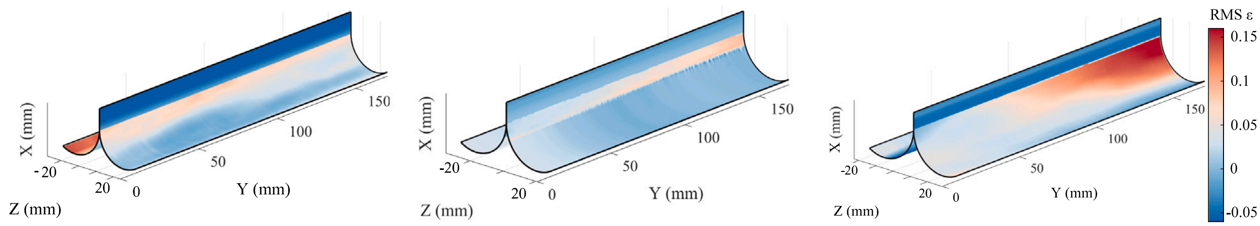

(a) FK longeron (b) SH longeron (c) XX longeron

Fig. 15. 3D scans of TRAC longerons made from different TP thin-ply prepreg systems in 3-step manufacturing process.

each sample was scanned using a Faro Arm Edge 14000 portable coordinate measurement system equipped with a 3D laser scanner. The longerons were suspended vertically from the edge of a table using adhesive to minimize gravity-induced deformation of the flanges during scanning. For each longeron, point clouds of approximately one million points were acquired to ensure sufficient resolution for accurate assessment of the surface geometry and flange curvature.

The analysis follows the method described by Benazzo and Pellegrino [30], in which best-fit cylinders are computed for both flanges and deviations from the ideal cylindrical shape are evaluated using the root-mean-square error (RMS ε):

$$\text{RMS } \varepsilon = \frac{\sqrt{(x - x_{\text{fit}})^2 + (z - z_{\text{fit}})^2} - \bar{r}}{\bar{r}} \tag{1}$$

Here, x and z denote the point cloud coordinates, x_{fit} and y_{fit} the coordinates of the closest point on the fitted cylinder, and $\bar{r}$ the mean radius of the fitted cylinder. RMS error contours are visualized in both 3D and 2D in Figs. 15–16. In the 3D plots, the full flange geometry is reconstructed to visualize overall deformation trends. In contrast, the 2D plots show the RMS deviation as a function of the subtended angle, ranging from 0° at the web–flange interface to 110° at the flange tip, enabling a more detailed comparison of the local shape accuracy.

The mean radii of the fitted cylinders for FK, XX, and SH are 14.00 mm, 17.25 mm, and 18.83 mm, respectively. Notably, the FK longeron exhibits the best geometric conformity, with a deviation of only 10.2% from the nominal mold radius of 12.7 mm. In contrast, the XX and SH longerons deviate from the nominal radius by 35.8% and 48.3%, respectively, indicating substantial spring-back. Benazzo and Pellegrino [30] report shape deviations of ≤7% from the mold radius for TP-based TRAC longerons manufactured via autoclave processing, which suggests that the larger spring-back observed here may stem from the lack of a more uniform autoclave pressure or from differences in thermal history and residual stress development in the 3-stage out-of-autoclave process. Nonetheless, considering the results of the FK longeron, the out-of-autoclave process is quite promising. Especially, when considering that shape deviations in thermoset TRAC longerongs manufactured in an autoclave process are around 8%, as recently reported in Carmi and Pellegrino [54]. Both in- and out-of-autoclave manufactured TP-based TRAC longerons exhibit spring-back rather than spring-in [30]. This is in contrast to the spring-in behavior reported for TS-based composite TRAC booms [15], where cure shrinkage and thermal mismatch cause inward shape distortion [40]. The more pronounced spring-back in XX and SH samples compared to FK is likely a result of higher residual thermal stresses and poorer through-thickness homogeneity. As shown in Fig. 3, the XX prepreg exhibits significant thickness variation and uneven fiber distribution. These material inconsistencies, combined with potential asymmetries during the ply stacking process, promote uneven stress build-up during cooling, which manifests as flange curvature deviation and web twist. In addition, differences in the molecular characteristics of the PEEK matrix (e.g. chain length or crystallization kinetics) may further influence the shape recovery. Higher molecular weight systems (as may be present in XX or SH) generally exhibit slower crystallization and retain more locked-in stress, especially when shaped at sub-optimal temperatures. The use of a uniform shaping temperature (365 °C) across all materials may thus lead to unequal stress relaxation behavior, depending on the resin formulation and fiber architecture.

The 2D RMS error plots in Fig. 16 provide detailed insight into the local shape deviations along the flanges. While the general shape accuracy of the FK longeron in terms of the nominal mean flange radius is good, there are noticeable differences between the left and right flanges. Most local deviations in Fig. 16(a) are within ±5%, indicating high geometric accuracy overall. However, the left flange shows slightly higher deviations near the outer edge, reaching up to 10%. Along the longitudinal axis, the deviation remains relatively uniform, with no visible signs of twist, aligning well with visual observations. In contrast, the XX longeron in Fig. 16(c) exhibits significantly larger deviations, ranging from −5% to +15% across wide regions. In addition, the deviations in the longeron are highly asymmetrical, which correlates with the twist seen in the physical specimen. For SH, although the mean flange radius deviates substantially from the nominal value (48.3%), the flange shape is comparatively uniform, with most local deviations within ±5%. However, asymmetry along the main axis is still present. Autoclave-cured TS TRAC longerons have been reported to exhibit web

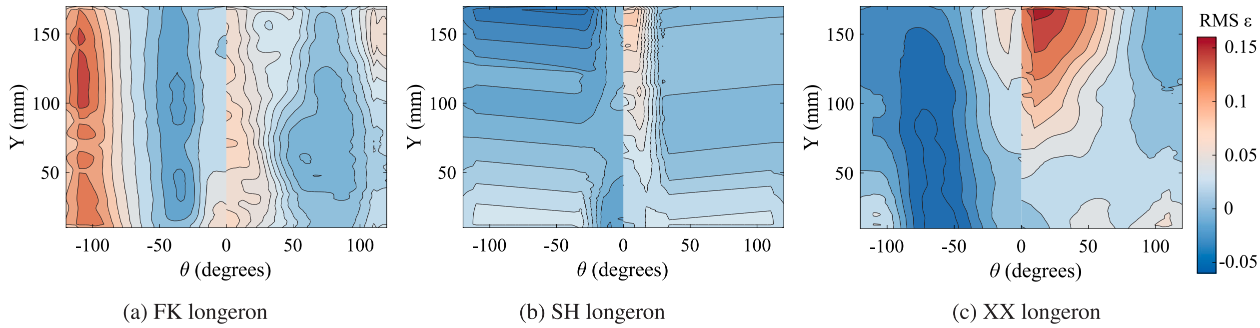

Fig. 16. 2D scans of flange area of TRAC longerons made from different TP thin-ply prepreg systems in 3-step manufacturing process.

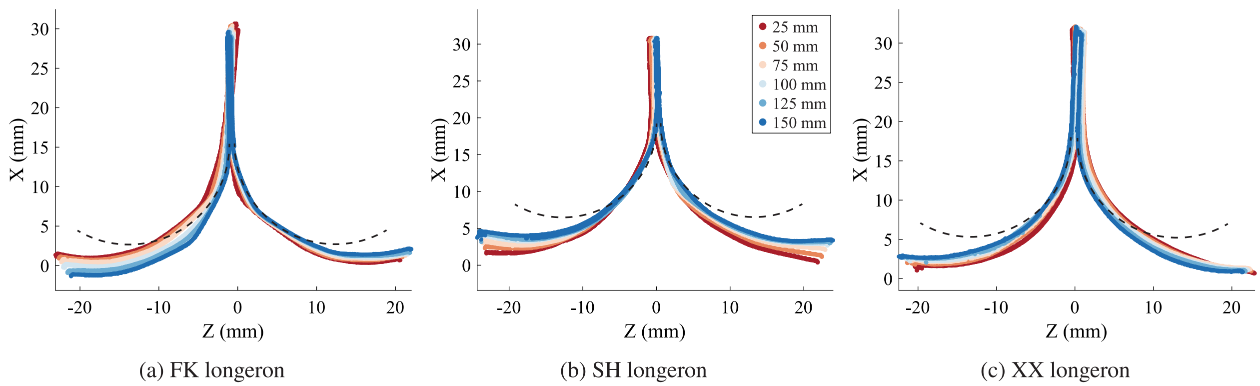

Fig. 17. Cross-sections of TRAC longerons made from different TP thin-ply prepreg systems in 3-step manufacturing process (outlined shape of the mold cross-section in dashed lines).

twists of up to 10° by Leclerc [55]. It is important to note, however, that the TS longerons investigated in that study were considerably longer (600 mm) than the present TP longerons (200 mm). While the twist in the present TP longerons appears notably smaller, caution is required in drawing direct comparisons given the limited comparability of the geometries.

To better illustrate the shape accuracy along the longitudinal axis, cross-sectional profiles extracted every 25 mm in the X–Z plane are presented in Fig. 17. The FK longeron most closely approximates the nominal flange curvature, however, subtle discrepancies between the left and right flanges are evident. In the case of XX, the flange curvature deviates substantially from the target radius, which is expected to result in non-uniform overall bending stiffness of the longeron. The SH specimen likewise exhibits a significant deviation from the nominal radius. In addition, asymmetries along the main axis are visible and appear to correlate with an increase in flange radius toward one end, further compromising shape accuracy and potentially affecting the structural performance of the component.

Overall, the FK prepreg shows the most favorable forming response, especially in terms of radial shape accuracy while structural symmetry leaves room for improvement. These findings underscore the importance of optimizing not only the consolidation parameters to minimize voids and improve impregnation (see Sections 2.2 and 2.3), but also the shaping temperature and dwell time to minimize the shape distortion. As TRAC longerons are scaled up to meter-class lengths, even moderate deviations in flange geometry or web alignment can accumulate and negatively impact their deployment behavior and structural efficiency. A deeper understanding of the interplay between prepreg characteristics, residual stresses, and shaping behavior is therefore essential for advancing reliable quasi-continuous manufacturing routes for ultra-thin composite space structures. In addition, future development stages might be further improved by taking advantage of tool-compensation techniques in order to counteract spring-in/back effects, as demonstrated by Kappel et al. [56] on open cross-section L-flanges.

3.3. Laminate quality

The internal microstructure of the TRAC longerons was examined using CT imaging of both the web–flange transition and the central web region, with a spatial resolution of 3.5 μm per pixel (see Fig. 18). The FK specimen displays a well-defined outer contour and a smooth transition between flanges and web, however, with a few voids visible in the flange area. The PEEK interleaving film was not discernible in the web region, suggesting good laminate integration. However, at the flange–web corner a small resin pocket was observed. Slight bulging on the inward side of the flanges may result from insufficient lateral constraint during forming. These observations align with the favorable handling characteristics and geometric accuracy discussed earlier (Sections 2.1 and 2.3) for the FK material.

In contrast, the XX longeron showed significant porosity in the transition region in Fig. 18(e), with large voids distributed throughout the laminae, likely a consequence of the inhomogeneous prepreg quality discussed in Sections 2.1 and 2.3. One particularly critical observation is the coincidence of voids with the flange–web transition area, leading to highly compromised local integrity. The central web region in Fig. 18(f) further confirms poor consolidation, with elevated void content primarily in the outer plies and deviations in both total and ply-level thickness. The reduced void content at the laminate midplane may be attributed to the additional PEEK film, which likely compensates for insufficient matrix infiltration. These microstructural issues are consistent with the quality of the prepreg material as well as flange waviness, and reduced shape fidelity observed for XX.

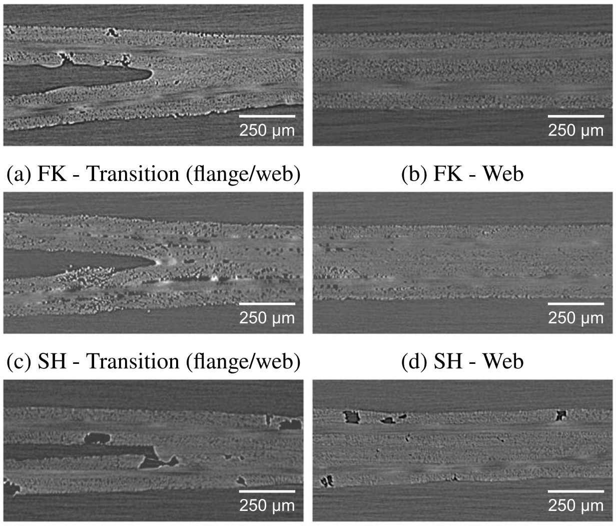

(a) FK - Transition (flange/web) (b) FK - Web

(c) SH - Transition (flange/web) (d) SH - Web

(e) XX - Transition (flange/web) (f) XX - Web

Fig. 18. CT scans of TRAC longerons at transition between web and flange area (left) and within web area (right).

The SH longeron shows a more differentiated pattern. The transition region in Fig. 18(c) is marked by low microstructural uniformity, fiber protrusions, fine-scale voids, and delamination. In contrast, the central web area in Fig. 18(d) exhibits markedly improved consolidation. Here, laminate and ply thicknesses are consistent, and void content is substantially reduced compared to the transition region. These findings correspond well with the visual and laser scan observations in Section 3.2, where the SH longeron exhibited uniform flange shape but significant spring-back and surface-level imperfections. The asymmetric consolidation behavior between web and transition regions in the SH longeron highlights the sensitivity of thin-ply CFRTP processing to local forming conditions and prepreg characteristics.

Together, these CT results reinforce the conclusion that prepreg quality, laminate homogeneity, and localized processing conditions directly impact both the mechanical performance and geometric precision of TRAC structures. Compared to TRAC longerons manufactured in an autoclave process using either TP thin-ply prepreg [30] or TS thin-ply prepreg [57], the present CT-based observations reveal increased microstructural variability in the out-of-autoclave specimens. While prior work reported clean web-flange transitions and low void content, several samples in this study, in particular XX and SH, exhibit significant porosity, resin-rich pockets, and fiber protrusions in the transition region. These defects are likely linked to a lack of normal pressure during welding as well as reduced lateral constraint during shaping and more variable consolidation inherent to press-based processing. Notably, the FK longeron demonstrates a relatively uniform and well-impregnated structure, approaching the quality achieved under autoclave conditions. When compared to TRAC structures made from TS thin-ply systems, the TP laminates examined here generally exhibit higher void content and lower interlaminar uniformity. This can be attributed to the higher melt viscosity and shorter processing windows of thermoplastic matrices, which make complete fiber wet-out more difficult-particularly in ultra-thin configurations. However, unlike thermoset systems, thermoplastics offer post-consolidation forming flexibility, which, if paired with improved prepreg quality, could enable defect-reduced processing in scalable out-of-autoclave methods.

3.4. Interface strength

After a qualitative assessment of the TRAC longerons in terms of shape accuracy (laser scanning) and laminate quality (CT imaging), a first evaluation of their mechanical performance was carried out. Since the laminate quality observed in Fig. 18 is expected to influence the interface strength in the web region, peel tests were conducted to probe the critical transition between flanges and web. For this purpose, the longerons were sectioned into 15 mm wide strips. To ensure smooth load introduction, 40 mm long strips of sandpaper with a 10 mm overlap were bonded to the open flange ends. Testing was performed on a Zwick/Roell Z005 universal testing machine equipped with a 5 kN load cell (see Fig. 19). The aim of these tests was to gain a better understanding of the TRAC specimens themselves rather than to establish standardized material properties. Accordingly, the procedure follows the general principles of ASTM D1876, but the specimens were not manufactured to meet the strict dimensional requirements of the standard.

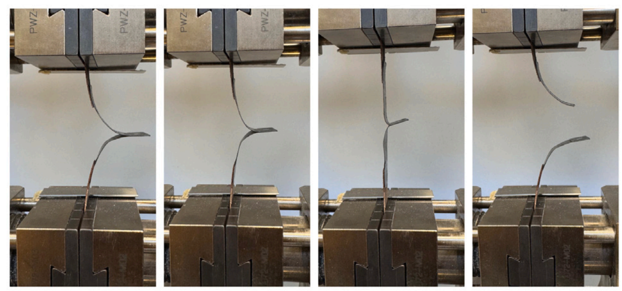

(a) Initial (b) Loading (c) Near F_{max} (d) Rupture

Fig. 19. Peel test of TRAC longeron section.

Fig. 20 presents the load–displacement curves obtained from peel tests on sections cut from the FK, SH, and XX longerons. For each longeron type, four specimens were tested. To improve clarity, the first 20 mm of displacement are omitted, as this regime corresponds to the initial loading phase characterized by large geometric compliance at low forces (see Figs. 19(a) and 19(b)). Because no steady-state peel plateau was observed in the force–displacement curves for the majority of specimens, peel strength is defined as the initiation peak peel force per unit width of the specimen ($S_{peel} = F_{max}/b$). The resulting values are summarized in Table 5.

The initial stiffness shows good repeatability, with curves for each material falling within a narrow band. The relative stiffness ranking across longeron types agrees with the tensile test results in Section 2.4. SH exhibits the highest stiffness, followed by FK and then XX. With respect to peel strength S_{peel}, FK and SH reach similar levels, whereas XX fails at markedly lower loads. The scatter in peel strength S_{peel} also reflects the laminate quality. Therein, materials with more homogeneous fiber distribution, e.g. FK, exhibit lower standard deviation and coefficient of variation, while those with higher inhomogeneity, e.g. SH, show increased variability. The link between laminate microstructure and crack growth behavior is examined in the following.

The fracture surfaces of the FK, SH, and XX sections were inspected after testing by optical microscopy, with representative examples shown in Fig. 21. The load–displacement curves exhibit a steep drop after reaching the maximum load, corresponding to rupture of the specimen (see Fig. 19(d)). In these cases, one of the flanges failed at the transition region between flange and web. Owing to the unfavorable layup with 90° plies at the web interface, interlaminar crack growth can easily transition into intralaminar cracking through the 90° ply. This weakens the flange laminate and ultimately causes flange rupture, as illustrated in Fig. 22.

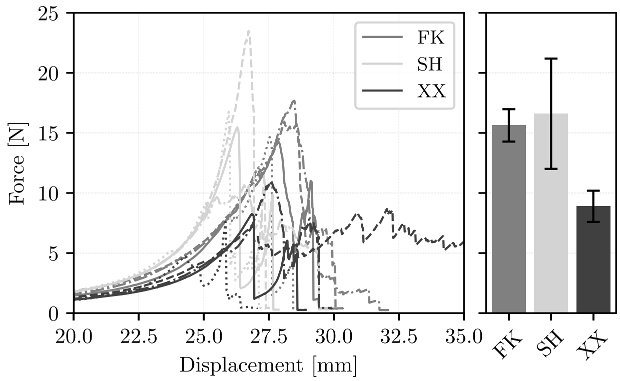

Fig. 20. Force–displacement curves of peel test incl. standard deviation for each material (FK, SH, XX).

Table 5
Peel strength S_{peel} for sections taken from TRAC longerons.

Material	Specimen	S_{peel} [N/mm]	Mean [N/mm]	Stdv. [N/mm]	CV [%]
FK	01	0.95	1.04	0.09	8.55
	02	1.06			
	03	1.18			
	04	0.98			
SH	01	1.03	1.11	0.31	27.63
	02	1.57			
	03	0.71			
	04	1.12			
XX	01	0.59	0.59	0.09	14.57
	02	0.58			
	03	0.74			
	04	0.51			

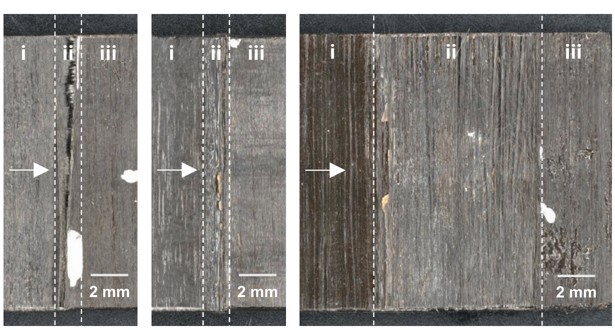

(a) FK-01 (b) SH-02 (c) XX-01

Fig. 21. Fracture surfaces after testing with crack growth direction indicated by arrow (i. flange surface, ii. inter-/intralaminar crack growth, iii. web surface)

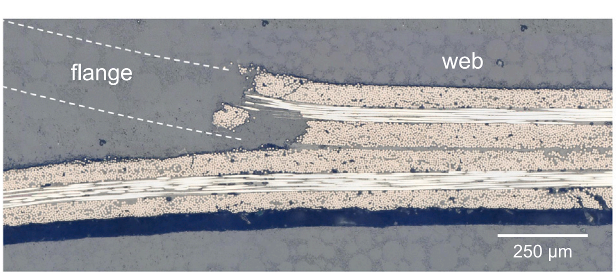

Fig. 22. Side view of FK-01 specimen at flange–web transition.

The transition from inter- to intralaminar crack planes is likely facilitated by defects in the flange/web region. As shown in Fig. 18, voids and delaminations are more prevalent in this area compared to the bulk of the web. Consistently, the fracture surfaces in Fig. 21 indicate that flange rupture typically occurs close to the flange/web transition, confirming the criticality of this region. These defects can arise from the lack of lateral support during the welding and shaping steps, as described in Section 3.3. Consequently, the peel tests highlight that improving the shaping process is essential to enhance the mechanical performance of the TRAC longeron, as only one specimen (XX-01) exhibited quasi-stable interlaminar crack propagation for a prolonged time.

While the present peel tests on sections taken from TRAC longerons provide a qualitative assessment of the mechanical performance of the flange/web transition and web interface, they do not constitute a comprehensive characterization of the interface behavior. A more rigorous quantification of fracture toughness would require dedicated interlaminar tests, such as double-cantilever-beam and end-notched flexure configurations [58], to capture delamination behavior in different modes and to determine the corresponding fracture toughness values. Nonetheless, the results correlate with the CT scans and prepreg fiber uniformity study, which identified the FK material as the most uniform prepreg tape. This underscores the importance of prepreg quality as a key parameter in thin composite manufacturing.

4. Conclusions

This study has demonstrated, for the first time, the manufacturing of ultra-thin thermoplastic TRAC longerons using a modular, out-of-autoclave process based on PEEK-based thin-ply prepreg systems. A 3-step manufacturing approach (comprising laminate consolidation, web welding, and flange shaping) has enabled the systematic investigation of key process parameters and their influence on laminate quality, mechanical performance, and shape accuracy. The main conclusions are summarized as follows:

- Among the evaluated prepreg systems, FK showed the most favorable combination of fiber distribution homogeneity, handling behavior, and final structural performance. XX exhibited the thinnest single-ply thickness but also the highest non-uniformity, which likely contributed to localized shape defects due to residual thermal stresses. SH showed better thickness uniformity but required elevated shaping temperatures to reduce spring-back. FK provided a balanced performance with moderate crystallinity and good uniformity, resulting in the most cylindrical flange shape.
- Shim thickness was identified as the most influential parameter governing laminate quality during processing. A shim thickness between 150–175 μm provided the best balance between dimensional stability, void suppression, and mechanical performance. Dwell temperature and dwell time primarily influences polymer crystallinity, which enhances stiffness but also increases residual stress and spring-back when not properly controlled. An optimized consolidation window of 395 °C, 3.5 MPa, and 30 min dwell time (405 °C for SH) was found to yield high-quality laminates with low void content and high shape fidelity, especially in case of FK.
- Mechanical testing revealed that laminates consolidated with thinner shims achieved higher stiffness and strength, though at the cost of increased scatter due to handling sensitivity and local fiber misalignment due to squeezing.
- Shape accuracy of the final TRAC longerons closely correlated with microstructural uniformity. Spring-back rather than spring-in was consistently observed, with flange deviations as high as 35%–48% for materials with higher inhomogeneity. CT imaging of the web and flange regions confirmed that high consolidation pressure and prepreg quality are essential to minimize void formation, interlaminar discontinuities, and geometric distortion.

- Peel tests further showed that defects on microscale critically affect the flange/web transition, where interlaminar cracks propagate into the neighboring 90° plies and lead to rupture of the flanges. The results highlight the need for improved lateral support during the shaping step to enhance the interface strength of TRAC longerons.

Overall, the results confirm that out-of-autoclave processing of ultra-thin thermoplastic laminates can approach autoclave-level quality, provided that material uniformity, consolidation pressure, and forming strategies are tightly controlled. This result paves the way for scalable, quasi-continuous manufacturing of deployable space structures without reliance on large autoclaves.

Building on these results, several aspects require further investigation to support process scaling, and increase robustness:

- As structural scales increase, tooling precision with sub-50 µm flatness and enhanced edge constraints will be critical to maintain laminate uniformity and shape stability.
- While each processing parameter was varied independently, the interaction of different parameters (e.g. high pressure at high temperature resulting in matrix squeeze-out) may play a significant role in shaping reliability and should be investigated in future design of experiment (DoE) based studies.
- Material-specific forming protocols, derived from DoE-based studies, including tailored shaping temperatures and dwell times for each prepreg type, may be necessary to minimize spring-back and ensure repeatability.
- Further improvements in prepreg manufacturing quality, particularly in tow spreading and impregnation uniformity, will be essential to fully exploit the forming flexibility offered by thermoplastic matrix systems.
- Structural-level mechanical performance and stowability are governed by the interplay between laminate thickness, stiffness, and bending strength. While the present work provides a phenomenological study focused on manufacturing, morphology, and shape accuracy, further work is needed to quantify the mechanical performance of thermoplastic TRAC longerons in terms of flexural stiffness, strength, and stowing capacity.

Therefore, it is believed that the development of robust, scalable, and flight-relevant out-of-autoclave manufacturing routes for next-generation thermoplastic deployable space systems is practically achievable.

CRediT authorship contribution statement

J. Koord: Writing – review & editing, Writing – original draft, Visualization, Validation, Methodology, Investigation, Formal analysis, Data curation, Conceptualization. **F. Benazzo:** Writing – review & editing, Visualization, Validation, Software, Methodology, Investigation, Formal analysis, Data curation, Conceptualization. **C. Hühne:** Writing – review & editing, Supervision, Resources, Project administration, Funding acquisition, Conceptualization. **S. Pellegrino:** Writing – review & editing, Supervision, Resources, Project administration, Methodology, Funding acquisition, Conceptualization.

Declaration of competing interest

The authors declare that they have no known competing financial interests or personal relationships that could have appeared to influence the work reported in this paper.

Acknowledgments

The authors acknowledge funding from the German Aerospace Center (DLR) through the project AMoCSiS (Automated Manufacturing of Composite Structures in Space) and from the Space Solar Power Project at Caltech. The authors also thank FUKUVI Chemical Industry Co., Ltd. and SHINDO Co., Ltd. for providing the thin-ply thermoplastic prepreg materials used in this study.

Data availability

Data will be made available on request.

References

[1] Leipold M, Runge H, Sickinger C. Large SAR membrane antennas with lightweight deployable booms. In: 28th ESA antenna workshop on space antenna systems and technologies. 2005.
[2] Campbell D, Barrett R, Lake M, Adams L, Abramson E, Scherbarthn M, Welsh J, Freebury G, Beidleman N, Abbot J. Development of a novel,passively deployed roll-out solar array. In: IEEE aerospace conference. 2006.
[3] Hoang B, White S, Spence B, Kiefer S. Commercialization of DeployableSpace systems' roll-out solar array (ROSA) technology for space systems loral (SSL) solar arrays. In: IEEE aerospace conference. 2011.
[4] Leipold M, Eiden M, Garner C, Herbeck L, Kassing D, Niederstadt T, Krüger T, Pagel G, Rezazad M, Rozemeijer WH, Seboldt W, Schöppinger C, Sickinger C, Unckenbold W. Solar sail technology development and demonstration. Acta Astronaut 2003;52:317–26.
[5] Banik J, Ardelean E. Verification of a retractable solar sail in a thermal vacuum environment. In: 51st AIAA/aSME/ASCE/AHS/aSC structures, structural dynamics, and materials conference. 2010.
[6] Rimrott F. Storable tubular extendible member: a unique machine element. Mach Des 1965;37(28):156–65.
[7] Aguirre-Martinez M, Bowen D, Davidson R, Lee R, Thorpe T. Thedevelopment of a continuous manufacturing method for a deployable satellitemast in CFRP. In: British plastics congress. 1986.
[8] Herbeck L, Leipold M, Sickinger C, Eiden M, Unckenbold W. Development and test of deployable ultra-lightweight cfrp-booms for a solar sail. In: Spacecraft Structures, Materials and Mechanical Testing. 2001,
[9] Fernandez J. Advanced deployable shell-based composite booms for smallsatellite structural applications including solar sails. In: 4th international symposium on solar sailing. Tokyo (Japan); 2017.
[10] Banik J, Murphey T. Performance validation of the triangular rollableand collapsible mast. In: Proceedings of the 24th annual AIAA/USu conferenceon small satellites. 2010.
[11] Roybal F, Banik J, Murphey T. Development of an elastically deployable boom for tensioned planar structures. In: 48th AIAA/aSME/ASCE/AHS/aSC structures, structural dynamics, and materials conference. 2007.
[12] Whorton M, Heaton A, Pinson G, Adams C. Nanosail-d: the first flight demonstration of solar sails for nanosatellites. In: 22nd AIAA/USu conferenceon small satellites. 2008.
[13] Johnson L, Whorton M, Heaton A, Pinson R, Laue G, Adams C. NanoSailD: a solar sail demonstration mission. Acta Astronaut 2011;68:571–5.
[14] Biddy C, Svitek T. LightSail-1 solar sail design and qualification. In: Proceedings of 41st aerospace mechanisms symposium. 2012.
[15] Leclerc C, Pellegrino S. Nonlinear elastic buckling of ultra-thin coilable booms. Int J Solids Struct 2020;203:46–56. http://dx.doi.org/10.1016/j.ijsolstr.2020.06.042.
[16] Fikes A, Gdoutos E, Klezenberg M, Ayling A, Mizrahi O, Sauder J, Sommer C, Truong A, Wen A, Wu A, Madonna R, Atwater H, Hajimiri A, Pellegrino S. The caltech space solar power demonstration one mission. In: 2022 IEEE international conference on wireless for space and extreme environments. IEEE; 2022, http://dx.doi.org/10.1109/wisee49342.2022.9926883.
[17] Sommer C, Gdoutos E, Truong A, Wen A, Sauder JF, Madonna R, Pellegrino S. Deployable on-orbit ultra-light composite experiment (DOLCE) on the caltech space solar power demonstration 1 (SSPD-1) mission. In: AIAA SCITECH 2025 forum. American Institute of Aeronautics and Astronautics; 2025, http://dx.doi.org/10.2514/6.2025-1007.
[18] Mallikarachchi HC, Pellegrino S. Dynamic analysis of large flat-foldable arrays – natural frequency bounds and influence of prestress. In: AIAA SCITECH 2025 forum. American Institute of Aeronautics and Astronautics; 2025, http://dx.doi.org/10.2514/6.2025-1194.
[19] Reznik S, Prosuntsov P, Mikhailovsky K, Shafikova I. Material science problems of building space antennas with a transformable reflector 100 m in diameter. IOP Conf Ser: Mater Sci Eng 2016;153:012001. http://dx.doi.org/10.1088/1757-899x/153/1/012001.

[20] Suh J-E, Dassanayake SP, Thomson M, Pellegrino S. Scalable concept for reflector antenna assembled in space. In: AIAA SCITECH 2024 forum. American Institute of Aeronautics and Astronautics; 2024, http://dx.doi.org/10.2514/6.2024-0823.

[21] Brown M, Tasker F, Kirby G. A deployable truss beam for long or lightly loaded space applications. In: 50th AIAA/aSME/ASCE/AHS/aSC structures, structural dynamics, and materials conference. American Institute of Aeronautics and Astronautics; 2009, http://dx.doi.org/10.2514/6.2009-2174.

[22] Schlothauer A. Resilient thin shell composites for extremely deformable structures [Ph.D. thesis], ETH Zürich; 2021.

[23] Leclerc C, Wilson LL, Bessa MA, Pellegrino S. Characterization of ultra-thin composite triangular rollable and collapsible booms. In: 4th AIAA spacecraft structures conference. American Institute of Aeronautics and Astronautics; 2017, http://dx.doi.org/10.2514/6.2017-0172.

[24] Glaser T, Richter M, Rege M, Orlowski-Feldhusen F, Mierheim O, Hühne C. Amocsis, on orbit manufacturing of composite truss structures. In: 16th ECSSMET 2021. 2021.

[25] Valente M, Rossitti I, Sambucci M. Different production processes for thermoplastic composite materials: Sustainability versus mechanical properties and processes parameter. Polymers 2023;15(1):242. http://dx.doi.org/10.3390/polym15010242.

[26] Nishida H, Carvelli V, Fujii T, Okubo K. Thermoplastic vs. thermoset epoxy carbon textile composites. IOP Conf Ser: Mater Sci Eng 2018;406:012043. http://dx.doi.org/10.1088/1757-899x/406/1/012043.

[27] Galos J. Thin-ply composite laminates: a review. Compos Struct 2020;236:111920. http://dx.doi.org/10.1016/j.compstruct.2020.111920.

[28] Schlothauer A, Pappas GA, Ermanni P. Thin-ply thermoplastic composites: From weak to robust transverse performance through microstructural and morphological tuning. Compos Part B: Eng 2023;261:110764. http://dx.doi.org/10.1016/j.compositesb.2023.110764.

[29] Gao S-L, Kim J-K. Cooling rate influences in carbon fibre/PEEK composites. Part 1. crystallinity and interface adhesion. Compos Part A: Appl Sci Manuf 2000;31(6):517–30. http://dx.doi.org/10.1016/s1359-835x(00)00009-9.

[30] Benazzo F, Pellegrino S. Design and manufacturing of ultra-thin thermoplastic composites for coilable longerons. In: AIAA SCITECH 2025 forum. Orlando, FL; 2025.

[31] Wang Y, Yang Y, Zhang H, Ding S, Yang T, Pang J, Zhang H, Zhang J, Zhang Y, Jiang Z. Study on the preparation and process parameter-mechanical property relationships of carbon fiber fabric reinforced poly(ether ether ketone) thermoplastic composites. Polymers 2024;16(7):897. http://dx.doi.org/10.3390/polym16070897.

[32] Li T, Song Z, Yang X, Du J. Influence of processing parameters on the mechanical properties of peek plates by hot compression molding. Materials 2022;16(1):36. http://dx.doi.org/10.3390/ma16010036.

[33] Lu C, Xu N, Zheng T, Zhang X, Lv H, Lu X, Xiao L, Zhang D. The optimization of process parameters and characterization of high-performance CF/PEEK composites prepared by flexible CF/PEEK plain weave fabrics. Polymers 2018;11(1):53. http://dx.doi.org/10.3390/polym11010053.

[34] Saenz-Castillo D, Martín M, Calvo S, Rodriguez-Lence F, Güemes A. Effect of processing parameters and void content on mechanical properties and NDI of thermoplastic composites. Compos Part A: Appl Sci Manuf 2019;121:308–20. http://dx.doi.org/10.1016/j.compositesa.2019.03.035.

[35] Hu J, Zhang H, Li S, Ji C, Chen S, Zhou Z, Wang B. Process parameter–mechanical property relationships and influence mechanism of advanced CFF/PEEK thermoplastic composites. Polym Compos 2022;43(8):5119–32. http://dx.doi.org/10.1002/pc.26801.

[36] Fujihara K, Huang Z-M, Ramakrishna S, Hamada H. Influence of processing conditions on bending property of continuous carbon fiber reinforced PEEK composites. Compos Sci Technol 2004;64(16):2525–34. http://dx.doi.org/10.1016/j.compscitech.2004.05.014.

[37] Stokes-Griffin C, Compston P. The effect of processing temperature and placement rate on the short beam strength of carbon fibre–PEEK manufactured using a laser tape placement process. Compos Part A: Appl Sci Manuf 2015;78:274–83. http://dx.doi.org/10.1016/j.compositesa.2015.08.008.

[38] Zheng B, Li M, Deng T, Zhou H, Huang Z, Zhou H, Li D. Process–structure–property relationships of thermoformed woven carbon-fiber-reinforced polyether-ether-ketone composites. Polym Compos 2019;40(10):3823–34. http://dx.doi.org/10.1002/pc.25241.

[39] Ye M, Lin F, Hu Y, Hu X. Enhanced mechanical properties of CF/PEEK and CF/Epoxy composites with micro-/nano- Aramid pulp interleaves. Compos Part A: Appl Sci Manuf 2025;196:108964. http://dx.doi.org/10.1016/j.compositesa.2025.108964.

[40] Parlevliet PP, Bersee HE, Beukers A. Residual stresses in thermoplastic composites – a study of the literature. Part III: Effects of thermal residual stresses. Compos Part A: Appl Sci Manuf 2007;38(6):1581–96. http://dx.doi.org/10.1016/j.compositesa.2006.12.005.

[41] Mehdikhani M, Gorbatikh L, Verpoest I, Lomov SV. Voids in fiber-reinforced polymer composites: A review on their formation, characteristics, and effects on mechanical performance. J Compos Mater 2018;53(12):1579–669. http://dx.doi.org/10.1177/0021998318772152.

[42] Parlevliet PP, Bersee HE, Beukers A. Residual stresses in thermoplastic composites—A study of the literature—Part I: Formation of residual stresses. Compos Part A: Appl Sci Manuf 2006;37(11):1847–57. http://dx.doi.org/10.1016/j.compositesa.2005.12.025.

[43] Phillips R, Glauser T, Månson JE. Thermal stability of PEEK/carbon fiber in air and its influence on consolidation. Polym Compos 1997;18(4):500–8. http://dx.doi.org/10.1002/pc.10302.

[44] Lu SX, Cebe P, Capel M. Thermal stability and thermal expansion studies of PEEK and related polyimides. Polymer 1996;37(14):2999–3009. http://dx.doi.org/10.1016/0032-3861(96)89397-9.

[45] Battes K, Day C, Hauer V. Outgassing behavior of different high-temperature resistant polymers. J Vac Sci Technol A: Vac Surfaces Films 2017;36(2). http://dx.doi.org/10.1116/1.5001243.

[46] Fayazbakhsh K, Abedian A. Materials selection for applications in space environment considering outgassing phenomenon. Adv Space Res 2010;45(6):741–9. http://dx.doi.org/10.1016/j.asr.2009.11.017.

[47] Kurtz SM. Chemical and radiation stability of PEEK. In: PEEK biomaterials handbook. Elsevier; 2012, p. 75–9. http://dx.doi.org/10.1016/b978-1-4377-4463-7.10006-5.

[48] Rival G, Paulmier T, Dantras E. Influence of electronic irradiations on the chemical and structural properties of PEEK for space applications. Polym Degrad Stab 2019;168:108943. http://dx.doi.org/10.1016/j.polymdegradstab.2019.108943.

[49] Kawabe K, Tomoda S, Matsuo T. Technology for spreading tow and its application to composite materials. Part 1. A new pneumatic method for spreading carbon tow. Sen'I Kikai Gakkaishi (J Textile Mach Soc Japan) 1997;50(3):T68–75. http://dx.doi.org/10.4188/transjtmsj.50.3_t68.

[50] Tardif X, Pignon B, Boyard N, Schmelzer JW, Sobotka V, Delaunay D, Schick C. Experimental study of crystallization of PolyEtherEtherKetone (PEEK) over a large temperature range using a nano-calorimeter. Polym Test 2014;36:10–9. http://dx.doi.org/10.1016/j.polymertesting.2014.03.013.

[51] Lu C, Xu C, Lu X, Ji W, Li S, Ma J, Ba S. Comparison and analysis of measurements for crystallinity of PEEK and CF/PEEK composites. Polym Compos 2024. http://dx.doi.org/10.1002/pc.29418.

[52] Seo J, Gohn AM, Dubin O, Takahashi H, Hasegawa H, Sato R, Rhoades AM, Schaake RP, Colby RH. Isothermal crystallization of poly(ether ether ketone) with different molecular weights over a wide temperature range. Polymer Crystallization 2019;2(1). http://dx.doi.org/10.1002/pcr2.10055.

[53] Ma X-l, Wen L-h, Wang S-y, Xiao J-y, Li W-h, Hou X. Inherent relationship between process parameters, crystallization and mechanical properties of continuous carbon fiber reinforced PEEK composites. Def Technol 2023;24:269–84. http://dx.doi.org/10.1016/j.dt.2022.04.010.

[54] Carmi MO, Pellegrino S. Manufacturing imperfections of open cross-section deployable thin-shell composite structures. In: AIAA SCITECH 2025 forum. American Institute of Aeronautics and Astronautics; 2025, http://dx.doi.org/10.2514/6.2025-0189.

[55] Leclerc C. Mechanics of ultra-thin composite coilable structures [Ph.D. thesis], California Institute of Technology (Caltech); 2020.

[56] Kappel E, Stefaniak D, Hühne C. Process distortions in prepreg manufacturing – An experimental study on CFRP L-profiles. Compos Struct 2013;106:615–25. http://dx.doi.org/10.1016/j.compstruct.2013.07.020.

[57] Hasanyan AD, Pellegrino S. Modeling of damage in coilable composite shell structures. In: AIAA SCITECH 2023 forum. American Institute of Aeronautics and Astronautics; 2023, http://dx.doi.org/10.2514/6.2023-0364.

[58] Hasanyan AD, Leclerc C, Pellegrino S. Interface failure analysis of triangular rollable and collapsible (TRAC) booms. In: AIAA scitech 2020 forum. American Institute of Aeronautics and Astronautics; 2020, http://dx.doi.org/10.2514/6.2020-0694.